iScience, Volume *27*

Supplemental information

Pseudouridine synthase 1 regulates erythropoiesis via transfer RNAs pseudouridylation and cytoplasmic translation

Deyang Shi, Bichen Wang, Haoyuan Li, Yu Lian, Qiuyi Ma, Tong Liu, Mutian Cao, Yuanwu Ma, Lei Shi, Weiping Yuan, Jun Shi, and Yajing Chu

Supplementary material

This supplementary material includes 9 supplementary figures

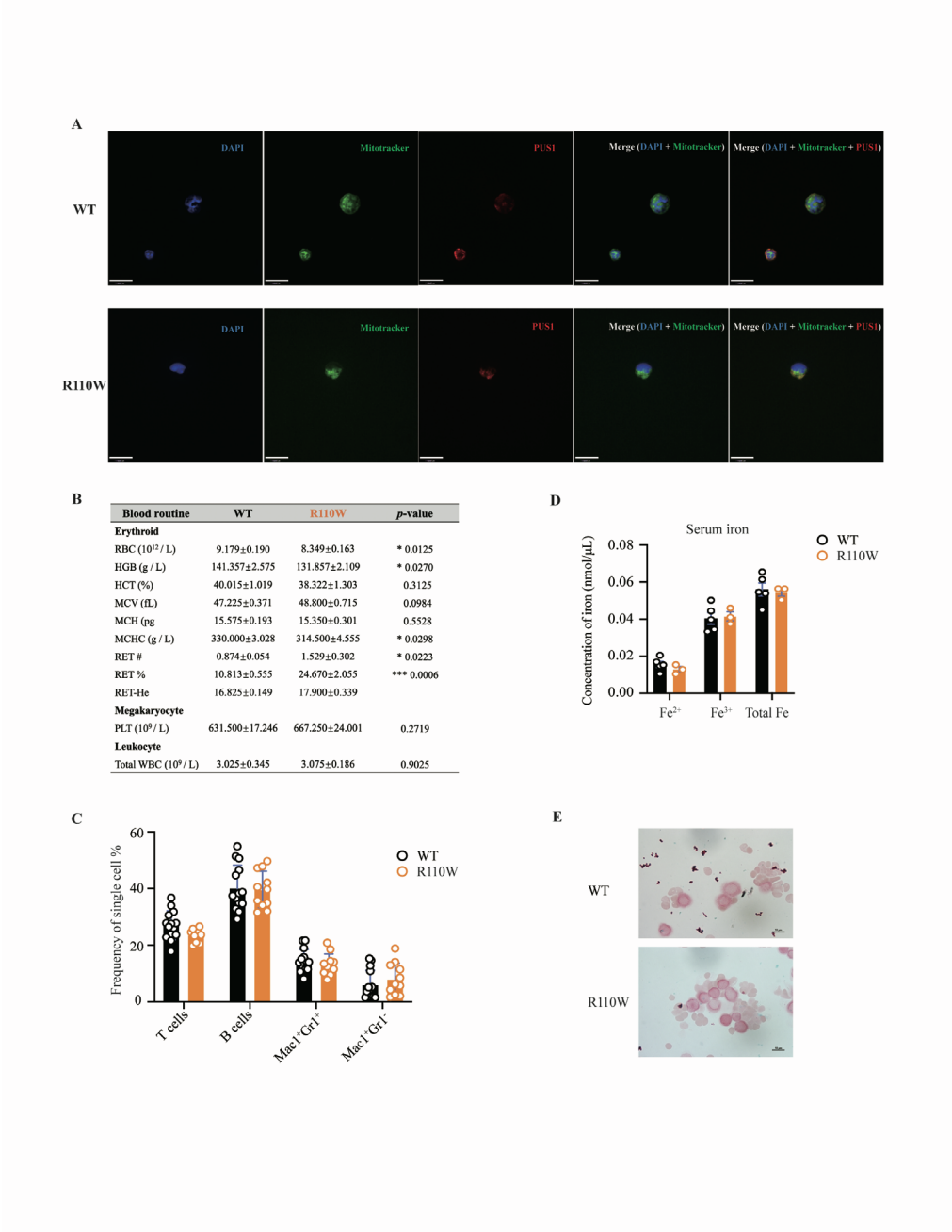

Blood routine	WT	R110W	*p*-value
Erythroid			
RBC (10^{12}/L)	9.179±0.190	8.349±0.163	* 0.0125
HGB (g/L)	141.357±2.575	131.857±2.109	* 0.0270
HCT (%)	40.015±1.019	38.322±1.303	0.3125
MCV (fL)	47.225±0.371	48.800±0.715	0.0984
MCH (pg	15.575±0.193	15.350±0.301	0.5528
MCHC (g/L)	330.000±3.028	314.500±4.555	* 0.0298
RET #	0.874±0.054	1.529±0.302	* 0.0223
RET %	10.813±0.555	24.670±2.055	*** 0.0006
RET-He	16.825±0.149	17.900±0.339	
Megakaryocyte			
PLT (10^9/L)	631.500±17.246	667.250±24.001	0.2719
Leukocyte			
Total WBC (10^9/L)	3.025±0.345	3.075±0.186	0.9025

Figure S1 Mutation in *Pus1* cause anemia without ring sideroblasts, related to Figure 1. (A) Co-localization of PUS1 with nucleus and mitochondria in mouse bone marrow cells by immunofluorescence (DAPI in blue; Mitotracker in green; PUS1 in red; Scale bars, 10 μm). (B) Complete blood routine of R110W and WT control mice (n=4). (C) The frequencies of $CD3^+$ T lymphocytes (T cells), $B220^+$ B lymphocytes (B cells), $Mac1^+Gr1^+$ and $Mac1^+Gr1^-$ myeloid cells in peripheral blood (n=14 for WT; n=11 for R110W). (D) Serum iron concentration in R110W and WT mice (n=5 for WT; n=3 for R110W). (E) Perl's staining of BM erythroblasts in R110W and WT mice (Scale bars, 10 μm). Data are represented as Mean ± SEM; * $P < 0.05$, ** $P < 0.01$, *** $P < 0.001$.

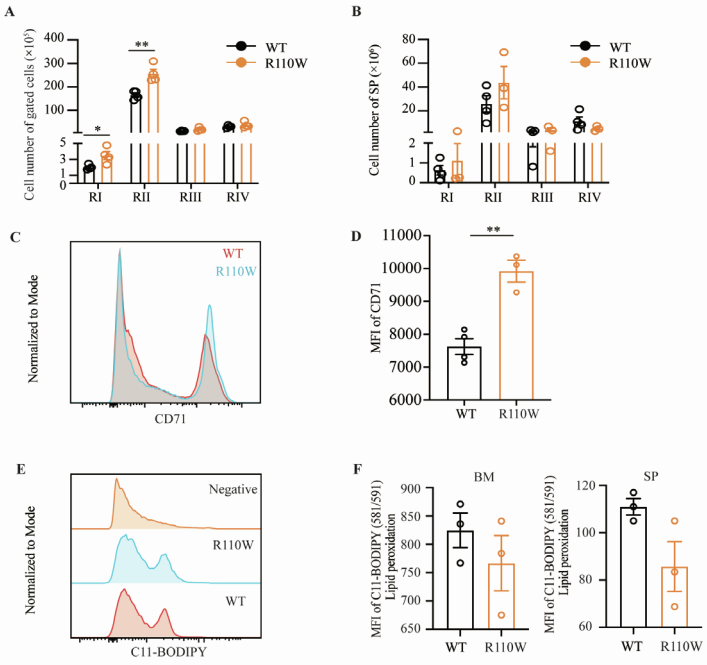

Figure S2 R110W mice impedes erythropoiesis in BM and spleen, related to Figure 2.
(A) The absolute cell number of erythroblasts in BM at different stages (n=4). (B) The absolute cell number of erythroblasts in spleen at different stages (n=4 for WT; n=3 for R110W). (C) MFI peak of CD71 in BM erythroblasts of the two groups. (D) MFI values of CD71 in BM erythroblasts of the two groups (n=4). (E) MFI peak of C11-BODIPY (581/591) (Lipid Peroxidation Sensor) in BM erythroblasts (n=3); Negative is the sample without sensor. (F) MFI values of C11-BODIPY (581/591) in BM erythroblasts (left, n=3). MFI values of C11-BODIPY (581/591) in spleen erythroblasts (right, n=3). Data are represented as Mean ± SEM; * P < 0.05, ** P < 0.01, *** P < 0.001.

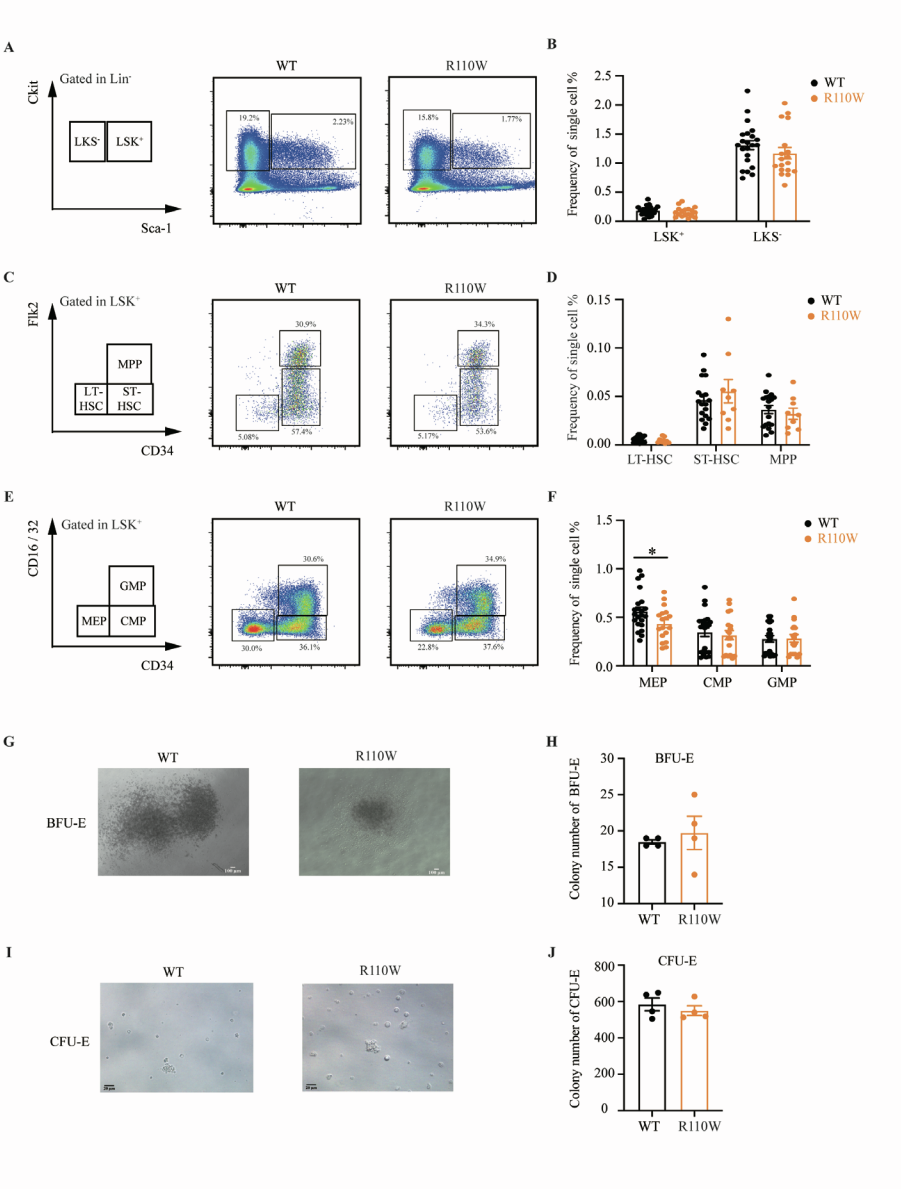

Figure S3 Effects of PUS1 on hematopoietic stem and progenitor cells, related to Figure 2.

(A) Flow cytometric gating strategy of LSK^+ and LKS^- cells in BM. (B) The proportion of LSK^+ and LKS^- cells in BM of R110W and WT control (n=22 for WT; n=18 for R110W). (C) Flow cytometric gating strategy of LT-HSC, ST-HSC and MPP cells in BM. (D) The proportion of long-term hematopoietic stem cells (LT-HSC), short-term hematopoietic stem cells (ST-HSC) and multipotent progenitor cells (MPP) cells in BM of R110W and control mice (n=18 for WT; n=9 for R110W). (E) Flow cytometric gating strategy of MEP, CMP and GMP cells in BM. (F) The proportion of megakaryocyte-erythroid progenitor cells (MEP), common-myeloid progenitor (CMP) and granulocyte-macrophage progenitor (GMP) cells in BM of R110W and control mice (n=22 for WT; n=18 for R110W). (G, I) Morphological characteristics of BFU-E (G, Scale bars, 100 μm) and CFU-E (I, Scale bars, 20 μm) differentiated from BM cells of R110W and control mice; Scale bars, 10 μm. (H, J) The colony counts of BFU-E (H) or CFU-E (J) differentiated from 4×10^4 BM cells (n=4). Data are represented as Mean ± SEM; * $P < 0.05$, ** $P < 0.01$, *** $P < 0.001$.

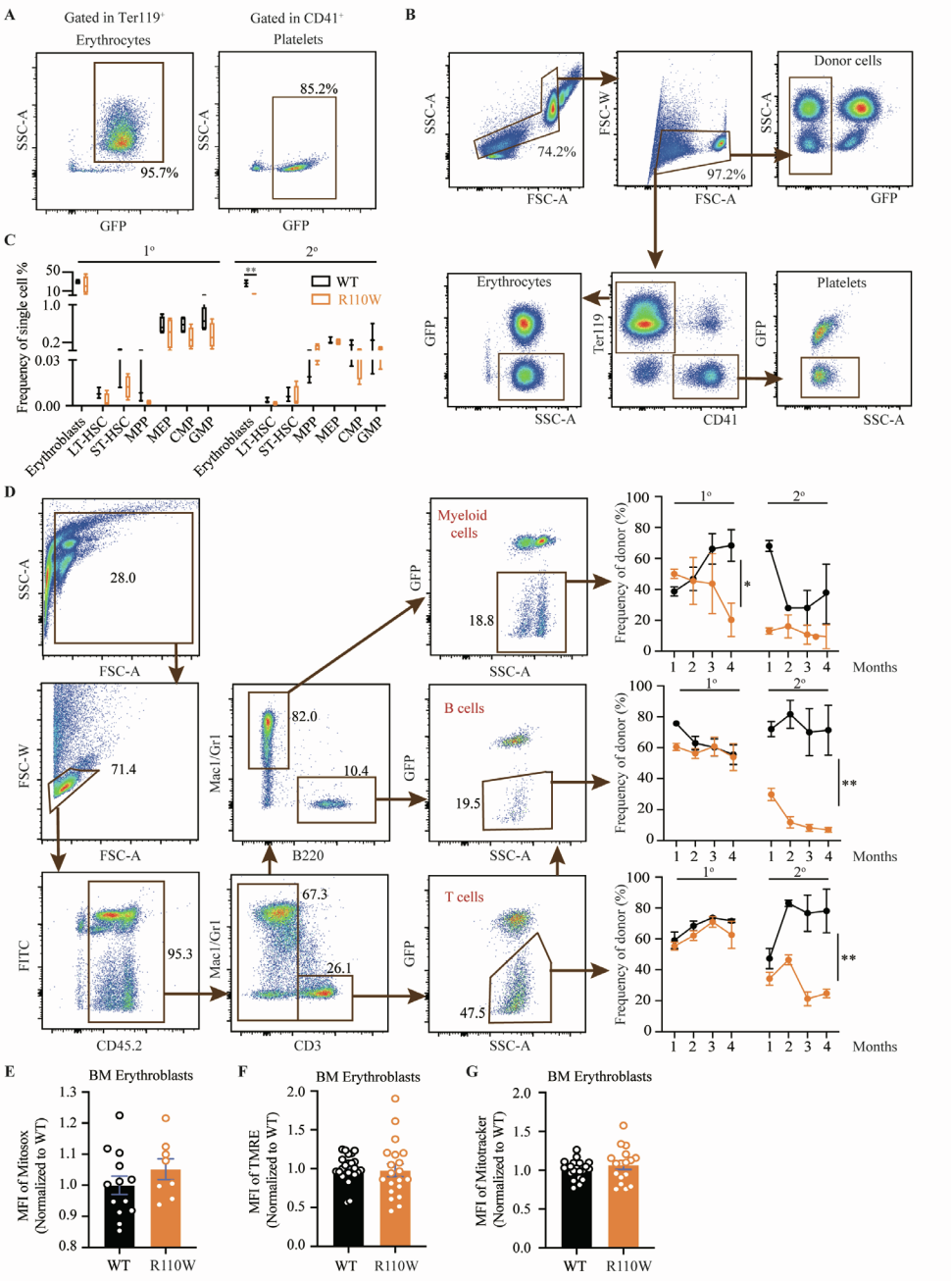

Figure S4 Analysis of donor derived cells in transplantation assay, related to Figure 2 and Figure 3.

(A) The proportion of GFP$^+$ erythrocytes and platelets in peripheral blood of actin-GFP mice. (B) Flow cytometric gating strategy to detect GFP− chimerism of platelets and erythrocytes in peripheral blood (PB). (C) Proportion of each lineage in donor derived BM cells (n=3 for WT; n=4 for R110W). (D) Flow cytometric gating strategy of donor derived GFP myeloid cells, T cells and B cells (left) and the frequency of donor derived GFP$^-$ cells (right, n=4). (E) MFI values of MitoSox in BM erythroblasts (n=20 for WT; n=16 for R110W). (F) MFI values of TMRE in BM erythroblasts (n=24 for WT; n=20 for R110W). (G) MFI values of Mitotracker in BM erythroblasts (n=22 for WT; n=17 for R110W). Data are represented as Mean ± SEM; * $P < 0.05$, ** $P < 0.01$, *** $P < 0.001$.

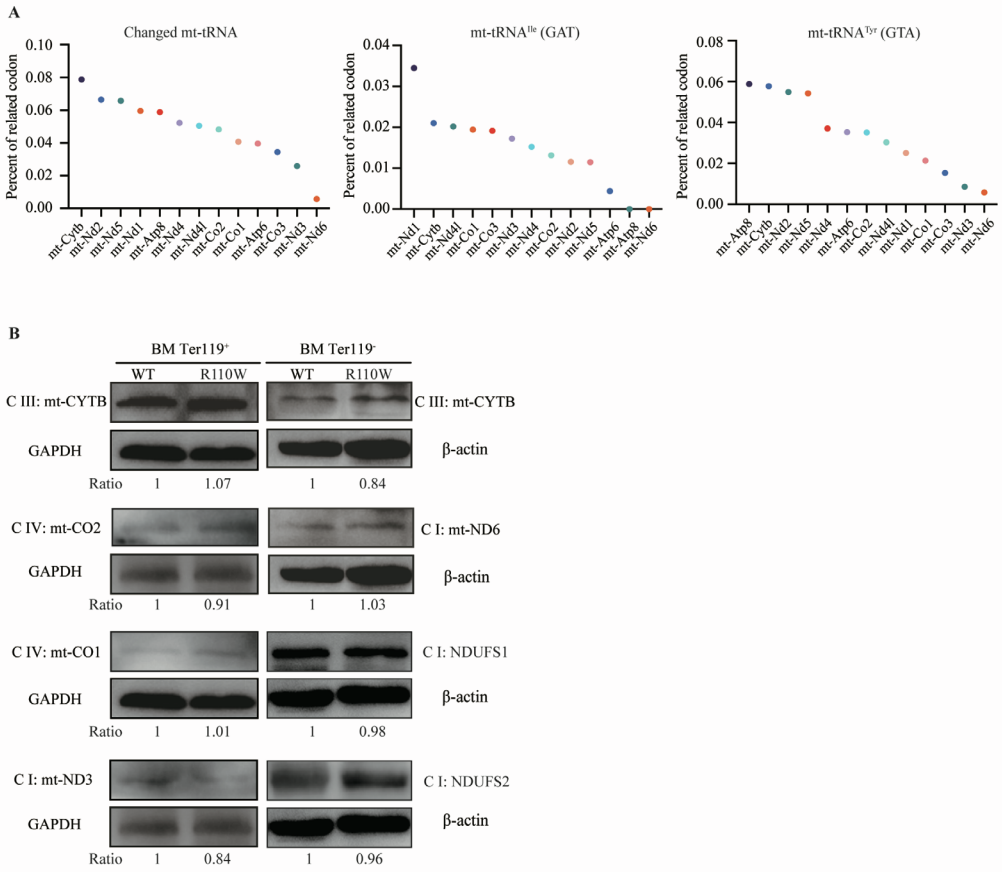

Figure S5 Changes in mitochondrial respiratory chain-related proteins caused by mutation in *Pus1*, related to Figure 4.

(A) Mitochondrial genome-encoded genes ranked by changed mitochondrial tRNAs (left), down-regulated mt-tRNA^{Ile} (GAT) (middle) and up-regulated mt-tRNA^{Tyr} (GTA) (right) corresponding codon frequencies. (B) Expression of mitochondrial OXPHOS protein level in BM Ter119^{+} erythroblasts (left) and Ter119^{-} non-erythroblasts (right) by Western blotting; mt-CYTB (complex III subunit), ND3 (complex I subunit), mt-CO1(complex IV subunit), mt-CO2 (complex IV subunit). The relative density was indicated.

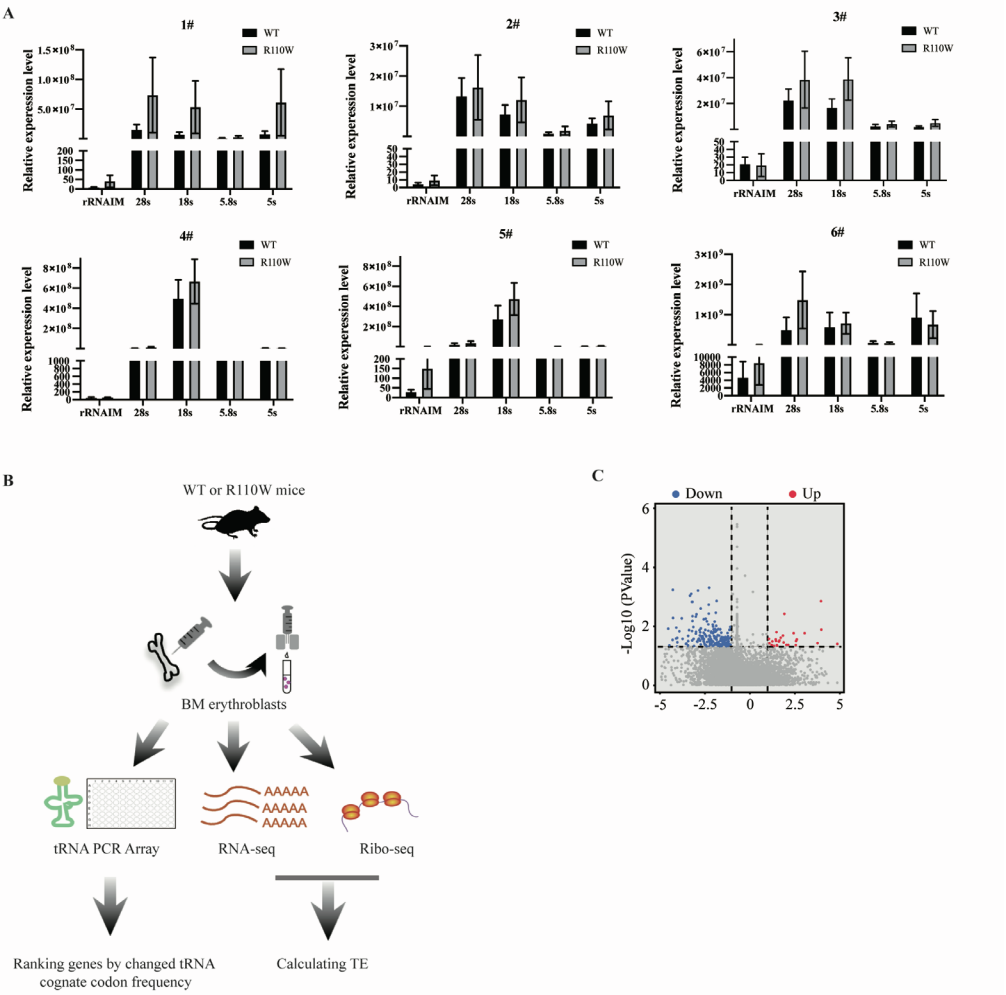

Figure S6. PUS1 mutation on translation may not be attributed to its effect on rRNA maturation of ribosome biogenesis, related to Figure 5.

(A) RNA from fractions 1 to 6 was extracted. The expression levels of mature and intermediate products of rRNA in samples tubes 1 to 6. (B) The experimental strategy of BM erythroblasts between two groups. (C) Volcano plot of differential TE genes between R110W and control BM erythroblasts (Fold Change > 2, $p < 0.05$, n=3). Blue, down-regulated genes; Red, up-regulated genes. TE for each transcript was calculated by dividing normalized ribosome-protected fragment reads (as assessed by Ribo-seq) by the normalized RNA-seq reads in the form of RPKM. Data are represented as Mean ± SEM; * $P < 0.05$, ** $P < 0.01$, *** $P < 0.001$.

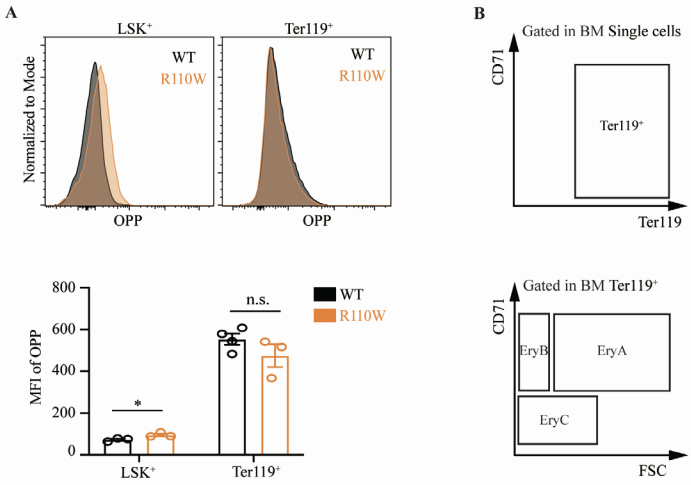

Figure S7 OPP incorporation in LSK$^+$ cells and Ter119$^+$ erythroblasts, related to Figure 5. (A) MFI values of OPP in BM LSK$^+$ cells and Ter119$^+$ erythroblasts (n=3). (B) Flow cytometric gating strategy of erythroblasts in BM by CD71 and Ter119 staining. EryA / B / C are gated in BM Ter119$^+$ erythroblasts. EryA: basophilic erythroblasts; EryB: polychromatophilic erythroblast; EryC: orthochromatic erythroblasts. Data are represented as Mean ± SEM; * P < 0.05, ** P < 0.01, *** P < 0.001.

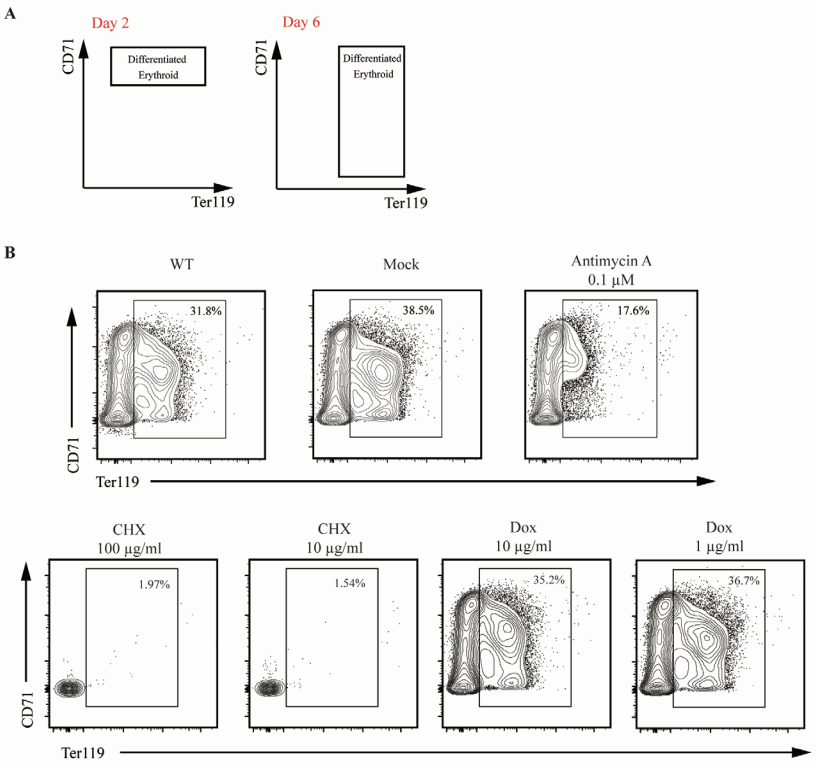

Figure S8 Flow cytometric analysis of *in vitro* erythroid differentiation, related to Figure 6.

(A) Flow cytometric analysis strategy of differentiated erythroblasts of *in vitro* erythroid differentiation. (B) Flow cytometric analysis of inhibitors on erythropoiesis *in vitro* at 6 days after differentiation. Inhibitors and their concentration are listed in the panels.

A

PUS1-dependent Ψ list in mRNAs and ncRNAs

References	Genes
Zhang M, Jiang Z, Ma Y, Liu W, Zhuang Y, Lu B, Li K, Peng J, Yi C. Quantitative profiling of pseudouridylation landscape in the human transcriptome. Nat Chem Biol. 2023 Oct;19(10):1185-1195. (PMID: 36997645)	RPL18A DNAJB12 RPS8 DCAF11 SLC35B2 CBR1 DDX52 LARP4B AGRN UNC13B KAT14 EIF3H UBE4A ENPP1 XPOT ARL5A SNRNP200 SH2B1 SELENON FOXRED2 TMX1 NFATC2IP FN1 RPL19P12 MRPS2 CBWD5 TM2D1 RPL37 PTPRF LAMA5 IPO5 SCAP CAPN1 LPCAT3 CLUH ANKFY1 CBWD2
Li X, Zhu P, Ma S, Song J, Bai J, Sun F, Yi C. Chemical pulldown reveals dynamic pseudouridylation of the mammalian transcriptome. Nat Chem Biol. 2015 Aug;11(8):592-7. (PMID: 26075521)	MLEC GNL3L VEZT GMPPA CDC45 TFDP1 PRKCSH RPL36A STAU1 TFIP11 PGRMC2 GIPC1 SRA1 BAG6 ZCCHC17 PYGB EEF1A1 HSPA9 EIF4E2 GLOD4 SLC35E1 MED1 PRRC2C ATF6 AP2S1 IPO4 CDC42 SHMT2 SETD5 ABCB7 CCT7 PCCB HYOU1 GET4 MSN R3HDM4 CLPTM1 MORF4L2 TFIP11 SLX1B AP2A2 NSUN2 SLC7A5 RBBP7 DYNC1LI2 LAP3 LARS2 DNAAF5 MRPS10 PCID2 TMEM126B MRPL4 HADH CHPT1 MIPEP BAD CHRNA7 MTRNR2L5 LRRC74B CXORF56 POLR1E COL18A1 ATP23 TSACC RIMKLA STAG3L4

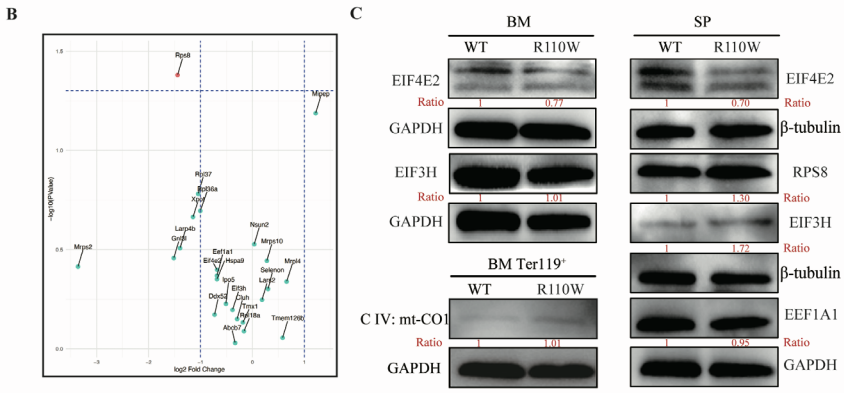

Figure S9 The reduced protein translation observed in PUS1 mutant cells was not related with PUS1 targeted mRNA coding genes involved in OXPHOS pathway or cytosolic protein regulation, related to Figure 6.

(A) PUS1-dependent Ψ list in mRNAs and ncRNAs. Genes potentially related to OXPHOS pathway or cytosolic protein regulation were highlighted in red. (B) Volcano plot of PUS1 targeted genes related to cytoplasmic protein regulation and oxidative stress response between the two groups. (C) Protein levels analysis by Western blot. The ratio represents the fold change in expression between the two groups as measured by densitometric analysis.